Oxidative Dehydrogenation of Propane over $V_2O_5/MoO_3/Al_2O_3$ and $V_2O_5/Cr_2O_3/Al_2O_3$: Structural Characterization and Catalytic Function

Shuwu Yang, Enrique Iglesia,* and Alexis T. Bell*

Chemical Sciences Division, Lawrence Berkeley National Laboratory, and Department of Chemical Engineering, University of California, Berkeley, California 94720-1462

Received: November 8, 2004; In Final Form: February 11, 2005

The structure and catalytic properties of binary dispersed oxide structures prepared by sequential deposition of VO_x and MoO_x or VO_x and CrO_x on Al_2O_3 were examined using Raman and UV−visible spectroscopies, the dynamics of stoichiometric reduction in H_2, and the oxidative dehydrogenation of propane. VO_x domains on Al_2O_3 modified by an equivalent MoO_x monolayer led to dispersed binary structures at all surface densities. MoO_x layers led to higher reactivity for VO_x domains present at low VO_x surface densities by replacing V−O−Al structures with more reactive V−O−Mo species. At higher surface densities, V−O−V structures in prevalent polyvanadates were replaced with less reactive V−O−Mo, leading to lower reducibility and oxidative dehydrogenation rates. Raman, reduction, and UV−visible data indicate that polyvanadates predominant on Al_2O_3 convert to dispersed binary oxide structures when MoO_x is deposited before or after VO_x deposition; these structures are less reducible and show higher UV−visible absorption energies than polyvanadate structures on Al_2O_3. The deposition sequence in binary Mo−V catalysts did not lead to significant differences in structure or catalytic rates, suggesting that the two active oxide components become intimately mixed. The deposition of CrO_x on Al_2O_3 led to more reactive VO_x domains than those deposited on pure Al_2O_3 at similar VO_x surface densities. At all surface densities, the replacement of V−O−Al or V−O−V structures with V−O−Cr increased the reducibility and catalytic reactivity of VO_x domains; it also led to higher propene selectivities via the selective inhibition of secondary C_3H_6 combustion pathways, prevalent in $VO_x-Al_2O_3$, and of C_3H_8 combustion routes that lead to low alkene selectivities on $CrO_x-Al_2O_3$. VO_x and CrO_x mix significantly during synthesis or thermal treatment to form $CrVO_4$ domains. The deposition sequence, however, influences catalytic selectivities and reduction rates, suggesting the retention of some of the component deposited last as unmixed domains exposed at catalyst surfaces. These findings suggest that the reduction and catalytic properties of active VO_x domains can be modified significantly by the formation of binary dispersed structures. VO_x-CrO_x structures, in particular, lead to higher oxidative dehydrogenation rates and selectivities than do VO_x domains present at similar surface densities on pure Al_2O_3 supports.

1. Introduction

The oxidative dehydrogenation (ODH) of propane provides an attractive route for the synthesis of propene.[1−15] This reaction occurs on oxides of V,[16−31] Mo,[19,23,38−44] and Cr,[39−46] with V-based catalysts typically providing higher rates and propene selectivities.[19,23] Supports influence rates and selectivities on dispersed VO_x domains.[17,20] For example, VO_x supported on ZrO_2[16,30,31] is highly active but gives low propene selectivities, while VO_x/Al_2O_3 gives lower rates but much higher alkene selectivities.[17,20]

ODH reactions on supported VO_x catalysts involve redox cycles and kinetically relevant C−H bond activation steps that require electron transfer from O to V within VO_x domains.[18,19,23,35,47] Chen et al.[23] showed that ODH turnover rates increase with decreasing VO_x UV−visible absorption edge energies and with increasing reducibility of VO_x domains in H_2. ODH turnover rates increased as polyvanadates became the predominant VO_x species, suggesting that linkages between monovanadate structures and support cations decrease the reactivity and reducibility of V−oxo species. These data also suggested that an intervening layer of a more reducible oxide (MO_x) may minimize these support effects by replacing V−O-support linkages with more reactive V−O−M linkages.

Few such binary dispersed oxide catalysts have been reported. Gao et al.[48] and Liu et al.[49] reported the catalytic properties of $V_2O_5/TiO_2/SiO_2$ for CH_3OH oxidation and $VO_x/SnO_x/Al_2O_3$ for CH_3OCH_3 oxidation, respectively. In both studies, the intervening layer increased the reducibility and catalytic activity of VO_x domains. Such binary dispersed structures have also been examined for ODH reactions. Cherian et al.[40] reported that VO_x structures on Al_2O_3 and TiO_2 supported modified by CrO_x gave higher rates but lower propene selectivities than catalysts containing only VO_x domains on these supports. The latter study reported a single composition, without systematic examination of any structural implications and catalytic consequences of compositional changes. Dai et al.[50] described a series of binary dispersed $VO_x/MoO_x/Al_2O_3$ catalysts prepared by dispersing VO_x on Al_2O_3 modified by a nominal polymolybdate monolayer. For a given VO_x surface density, active structures on MoO_x-coated Al_2O_3 were more reducible than those on Al_2O_3, apparently because less reactive V−O−Al linkages are replaced with V−O−Mo bonds; these trends were also reflected in the higher propane ODH turnover rates measured on VO_x structures

* Corresponding authors. E-mail: bell@cchem.berkeley.edu (A.T.B.); iglesia@cchem.berkeley.edu (E.I.).

10.1021/jp040708q CCC: $30.25
Published on Web 03/29/2005

dispersed in MoO_x/Al_2O_3 relative to those on similar VO_x domains on pure Al_2O_3 supports. MoO_x interlayers also decreased primary and secondary combustion rates and led to higher propene selectivities. In contrast, Bañares and Khatib[51] found no synergistic effects in VO_x-MoO_x/Al_2O_3 samples prepared by coimpregnation, which contained Mo−V−O mixed phases at (Mo + V) surface densities above those required for two-dimensional oxo-oligomers on Al_2O_3 surfaces.

Here, we aim to probe the structure and catalytic function of binary dispersed oxide catalysts for alkane ODH reactions. Samples were prepared by dispersing VO_x species on Al_2O_3 support surfaces modified by Mo and Cr oxides and also by preparing "inverse bilayers", in which Mo and Cr oxides are dispersed on Al_2O_3 modified by a polyvanadate monolayer. The resulting structures were examined by Raman and UV−visible spectroscopies and by measurements of their reduction dynamics in H_2, and their catalytic function was determined by rigorous measurements of turnover rates and of rate constants for primary and secondary reactions.

2. Experimental Section

2.1. Synthesis of Binary Dispersed Structures on Al_2O_3. Fumed Al_2O_3 (Degussa AG; surface area 107 m^2/g) was contacted with deionized water, dried at 383 K for 72 h, and treated in ambient air at 823 K for 3 h before use in a process intended to strengthen aggregates; its BET surface area was 125 m^2/g after this treatment. MoO_x/Al_2O_3 (MoAl) and CrO_x/Al_2O_3 (CrAl) with various active oxide surface densities were prepared by impregnating Al_2O_3 with solutions of molybdenyl acetylacetonate (Alfa Aesar, 99%) in acetone (Aldrich, 99.5%) or with aqueous solutions of chromium(III) nitrate nonahydrate (Aldrich, 98%). Samples were then dried at 383 K in ambient air overnight and treated in flowing dry air (Airgas, zero grade, 3.33 cm^3 s^{-1}) by heating to 773 K at 0.167 K s^{-1} and then holding at 773 K for 2 h. VO_x/Al_2O_3 (VAl) was prepared by incipient-wetness impregnation of Al_2O_3 with 2-propanol (Aldrich, 99.99%) solutions of vanadyl isopropoxide (Aldrich, 98%); samples were kept in a N_2 flow within a glovebox overnight and transferred into a quartz reactor sealed with stopcocks at each end. These samples were treated at 393 K in flowing N_2 (Airgas, 99.999%, 1.67 cm^3 s^{-1}) for 1 h and at 573 K for 1 h; air (Airgas, zero grade, 1.67 cm^3 s^{-1}) was then introduced and samples were held at 573 K for 1 h and at 773 K for 2 h.

Binary dispersed $VO_x/MoO_x/Al_2O_3$ (VMoAl) and $VO_x/CrO_x/Al_2O_3$ (VCrAl) catalysts were prepared by incipient-wetness impregnation of MoAl or CrAl samples with 2-propanol solutions of vanadyl isopropoxide with the same procedures used for VAl. $MoO_x/VO_x/Al_2O_3$ (MoVAl) catalysts with varying MoO_3 contents were prepared by impregnation of $10\%V_2O_5/Al_2O_3$ with acetone solutions of molybdenyl acetylacetonate, and then treating them at 383 K in ambient air and in flowing dry air at 773 K for 2 h. A $12\%Cr_2O_3/10\%V_2O_5/Al_2O_3$ (12Cr10VAl) sample was prepared by incipient-wetness impregnation of $10\%V_2O_5/Al_2O_3$ with aqueous chromium(III) nitrate solutions, followed by drying at 383 K in ambient air and treatment in flowing dry air at 773 K for 2 h.

2.2. Catalyst Characterization. BET surface areas were measured using Quantasorb units (Quantasorb 1 or Quantasorb 6 Surface Analyzers, Quantachrome Corp.) and N_2 at its normal boiling point. Samples were treated in dynamic vacuum (0.1 Pa) at 393 K for at least 3 h before BET measurements. X-ray diffraction (XRD) data were measured with a Siemens D5000 unit at ambient temperature using Cu Kα radiation. The X-ray tube was operated at 45 kV and 35 mA, and the scan rate was 1.2°/min.

Raman spectra were collected using a Hololab Series 5000 spectrometer (Kaiser Optical) equipped with a frequency-doubled 75-mW Nd:YAG laser (532 nm). Samples were pressed into self-supported wafers (0.9 cm diameter, ~50 mg cm^{-2}) at 200 MPa and then held onto a rotating holder within a quartz Raman cell. Raman spectra were recorded at ambient temperature before and after treating samples in flowing dry air (Airgas, zero grade, 0.83 cm^3 s^{-1}) while heating to 673 K at 0.167 K s^{-1} and holding at 673 K for 1 h.

Temperature-programmed reduction (TPR) studies were carried out in a flow unit (QS-10, Quantachrome Corp.). H_2 concentrations were measured using a thermal conductivity detector calibrated by reducing CuO. The sample amount (15−100 mg) was chosen to maintain a constant number of removable oxygen atoms (equivalent to 5 mg of MoO_3). Samples were heated to 1173 K in $20\%H_2-Ar$ (Praxair, 99.999%) at 0.167 K s^{-1} and held at 1173 K for 1 h. H_2O reduction products were removed before thermal conductivity detection with a 13X sieve at ambient temperature.

Diffuse reflectance UV−visible spectra were collected with a Cary 4 spectrophotometer (Varian Corp.) equipped with a Harrick Scientific diffuse reflectance attachment (DRP-XXX) and an environmental chamber (DRA-2CR). Samples were treated in 20% O_2−He (Praxair, 99.999%, 0.83 cm^3 s^{-1}) at 723 K for 0.5 h before measurements. The Kubelka−Munk function ($F(R_\infty)$) was used to convert reflectance data into pseudoabsorbance using MgO as a reflective standard.[52,53] Absorption-edge energies were calculated from the x-intercept of a linear regression of $[(F(R_\infty))h\nu]^{1/2}$ data versus $h\nu$.[53]

2.3. Catalytic Rates and Selectivity Measurements. Oxidative dehydrogenation rates and selectivities were measured at 583−673 K using a quartz flow microreactor. The reactor is 50 cm long, and the catalyst section is 10 mm in diameter and 35 mm in length. The reactor was heated via an electrical furnace, and the temperature was set by a temperature controller (WATLOW) and measured by a K-type thermocouple inserted into the reactor and positioned within the catalyst bed. Temperature gradients were avoided by diluting catalyst samples (20−40 mg, 250−500 μm) with equal amounts of acid-washed quartz (250−500 μm). C_3H_8 (13.5 kPa, Airgas, 99.9%) and O_2 (1.7 kPa, Airgas, 99.999%) with He as balance (Airgas, 99.999%) were used as reactants. C_3H_8 and O_2 conversions were kept below 2% and 20%, respectively, by varying reactant flow rates. Space velocities were 30 000−500 000 cm^3 g^{-1} h^{-1}. Reactant and product concentrations were measured by chromatography (Hewlett-Packard 6890) using a Carboxen 1004 packed column connected to a thermal conductivity detector and HP-PLOT Q capillary column with a flame ionization detector.

Reactor residence time effects on rates and selectivities were used to estimate C_3H_8 dehydrogenation (r_1) and combustion (r_2) rates by extrapolating C_3H_6 and CO_x synthesis rates to zero residence time. C_3H_6 combustion rates (r_3) were obtained from the slope of C_3H_6 selectivity data as a function of residence time.[16−23] These primary and secondary reactions and their respective rate constants (k_1, k_2, k_3) are shown in the scheme below:

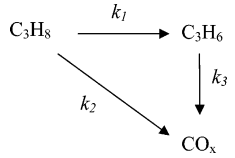

Dehydrogenation and combustion rates are assumed to be first-order in C_3H_8 and C_3H_6 and zero-order in O_2, as found

TABLE 1: BET Surface Areas and VO_x Surface Density of V_2O_5/Al_2O_3 Catalysts

catalyst	denotation	wt % V_2O_5[a]	surface area (m^2/g cat)	surface area (m^2/g Al_2O_3)	VO_x surface density (V/nm^2)
$3\%V_2O_5/Al_2O_3$	3VAl	3.1	108.1	111.6	1.9
$7\%V_2O_5/Al_2O_3$	7VAl	7.3	119.3	128.7	4.1
$10\%V_2O_5/Al_2O_3$	10VAl	8.3	103.3	112.6	5.3
$15\%V_2O_5/Al_2O_3$	15VAl	12.4	94.8	108.3	8.7
$18\%V_2O_5/Al_2O_3$	18VAl	14.8	91.1	106.9	10.7

[a] Weight loading obtained by inductively coupled plasma (ICP) analysis.

TABLE 2: BET Surface Areas and VO_x Surface Density of $V_2O_5/MoO_3/Al_2O_3$ and $MoO_3/V_2O_5/Al_2O_3$ Catalysts

catalyst	denotation	wt % V_2O_5	surface area (m^2/g cat)	surface area (m^2/g Al_2O_3)	VO_x surface density (V/nm^2)
$12\%MoO_3/Al_2O_3$	12MoAl		99.4	113.0	5.0 (Mo/nm^2)
$3\%V_2O_5/12\%MoO_3/Al_2O_3$	3V12MoAl	2.2[a]	90.1	104.7	1.6
$7\%V_2O_5/12\%MoO_3/Al_2O_3$	7V12MoAl	6.1[a]	90.8	109.8	4.4
$10\%V_2O_5/12\%MoO_3/Al_2O_3$	10V12MoAl	8.4[a]	81.2	100.7	6.9
$15\%V_2O_5/12\%MoO_3/Al_2O_3$	15V12MoAl	12.4[a]	84.6	109.8	9.7
$10\%V_2O_5/2\%MoO_3/Al_2O_3$	10V2MoAl	8.4[b]	105.5	117.4	5.3
$10\%V_2O_5/4\%MoO_3/Al_2O_3$	10V4MoAl	8.4[b]	89.9	102.2	6.2
$10\%V_2O_5/8\%MoO_3/Al_2O_3$	10V8MoAl	8.4[b]	83.8	99.4	6.6
$10\%V_2O_5/16\%MoO_3/Al_2O_3$	10V16MoAl	8.4[b]	77.3	100.4	7.2
$10\%V_2O_5/20\%MoO_3/Al_2O_3$	10V20MoAl	8.4[b]	74.5	101.6	7.5

[a] Weight loading obtained by inductively coupled plasma (ICP) analysis. [b] Assuming that 10V*x*MoAl has the same V_2O_5 loading as 10V12MoAl.

TABLE 3: BET Surface Areas and VO_x Surface Density of $V_2O_5/Cr_2O_3/Al_2O_3$ Catalysts

catalyst	denotation	wt % V_2O_5	surface area (m^2/g cat)	surface area (m^2/g Al_2O_3)	VO_x surface density (V/nm^2)
$12\%Cr_2O_3/Al_2O_3$	12CrAl		120.0	136.4	7.9 (Cr/nm^2)
$1\%V_2O_5/12\%Cr_2O_3/Al_2O_3$	1V12CrAl	1.0[a]	112.6	129.2	0.6
$3\%V_2O_5/12\%Cr_2O_3/Al_2O_3$	3V12CrAl	3.0[a]	94.8	111.1	2.1
$7\%V_2O_5/12\%Cr_2O_3/Al_2O_3$	7V12CrAl	6.4[a]	98.6	119.7	4.3
$10\%V_2O_5/12\%Cr_2O_3/Al_2O_3$	10V12CrAl	8.9[a]	93.0	116.0	6.3
$12\%V_2O_5/12\%Cr_2O_3/Al_2O_3$	12V12CrAl	10.4[a]	91.6	116.2	7.5
$15\%V_2O_5/12\%Cr_2O_3/Al_2O_3$	15V12CrAl	12.8[a]	90.5	117.9	9.4
$10\%V_2O_5/1\%Cr_2O_3/Al_2O_3$	10V1CrAl	8.9[b]	106.3	117.8	5.5
$10\%V_2O_5/3\%Cr_2O_3/Al_2O_3$	10V3CrAl	8.9[b]	105.5	119.3	5.6
$10\%V_2O_5/6\%Cr_2O_3/Al_2O_3$	10V6CrAl	8.9[b]	91.7	107.1	6.4
$10\%V_2O_5/9\%Cr_2O_3/Al_2O_3$	10V9CrAl	8.9[b]	96.5	116.4	6.1
$10\%V_2O_5/15\%Cr_2O_3/Al_2O_3$	10V15CrAl	8.9[b]	90.5	116.8	6.5

[a] Weight loading obtained by inductively coupled plasma (ICP) analysis. [b] Assuming that 10V*x*CrAl has the same V_2O_5 loading as 10V12CrAl.

experimentally on MoO_x and VO_x catalysts.[16−21] Values of k_2/k_1 are calculated from primary selectivities ($S_{C_3H_6}{}^0$) using

$$S_{C_3H_6}{}^0 = k_1/(k_1 + k_2)$$

while k_3 is obtained from C_3H_6 selectivities using

$$S_{C_3H_6} = S_{C_3H_6}{}^0[1 - (k_1 + k_2 + k_3)C_v\tau/2]$$

where τ is the residence time and C_v is the number of V-atoms per unit volume.[17]

3. Results and Discussion

3.1. Catalyst Characterization. *3.1.1. Surface Areas and Structure of Catalysts.* Surface areas and VO_x surface densities for all samples, as well as their designated nomenclature, are shown in Tables 1−3. Surface areas of VAl samples decreased with increasing VO_x content and surface density (Table 1), as was also found for VO_x dispersed on Al_2O_3 containing a nominal monolayer of MoO_x (12MoAl) or CrO_x (12CrAl). Surface areas for VMoAl and VCrAl with similar VO_x surface densities but varying MoO_x or CrO_x contents also decreased with increasing MoO_x and CrO_x content (Tables 2 and 3). These changes in surface areas merely reflect the larger total mass of samples per amount of Al_2O_3 in each sample; surface areas per amount of Al_2O_3 (Tables 1−3) are essentially the same in all samples. Thus, dispersing active oxides, as monolayers or bilayers, does not influence Al_2O_3 surface area.

Figure 1 shows X-ray diffraction data for selected samples. Pure Al_2O_3 shows only lines for its γ-phase, which is the only phase detected in 10VAl, 12MoAl, and 12CrAl. 10V12MoAl and 12Mo10VAl showed lines for $AlVMoO_7$ and weaker lines for $Mo_6V_9O_{40}$ and MoV_2O_8. Only γ-Al_2O_3 was detected in 10V12CrAl and 12Cr10VAl.

Figure 2 shows Raman spectra at ambient temperature for VAl samples with a range of VO_x surface densities treated in flowing dry air at 673 K for 1 h, and denoted as dehydrated samples throughout. The band at 1033 cm^{-1} was assigned to V═O stretches in monovanadates and polyvanadates, and the broad 750−1000 cm^{-1} bands were assigned to V−O−V stretches in two-dimensional polyvanadates.[20,22,54−56] Crystalline V_2O_5 gives sharp intense Raman bands at 1002, 708, 535, 490, 410, 305, 289, 203, and 150 cm^{-1}.[2] At low VO_x surface densities (1.9 V/nm^2), the ratio of the 1033 cm^{-1} band intensity (V═O stretch) to that for the 946 cm^{-1} band (V−O−V stretch) is high, indicating that monovanadates predominate on these samples.

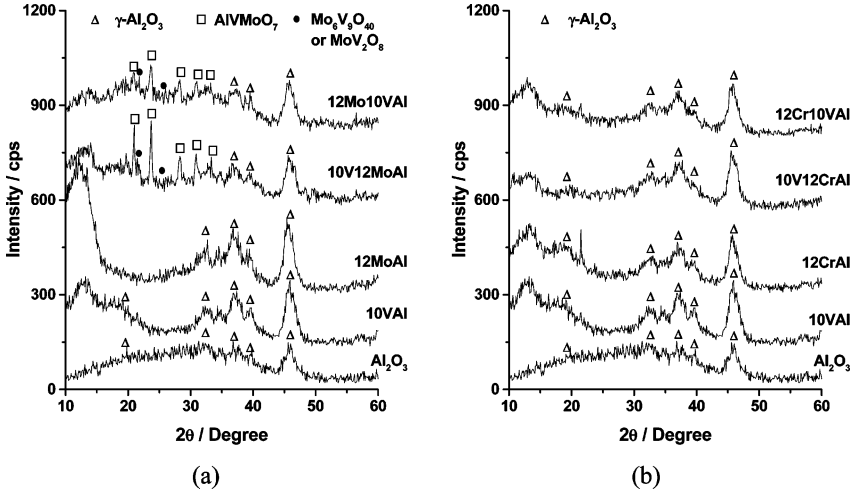

Figure 1. XRD patterns of (a) Al_2O_3, 10VAl, 12MoAl, 10V12MoAl, and 12Mo10VAl and (b) Al_2O_3, 10VAl, 12CrAl, 10V12CrAl, and 12Cr10VAl. Assignments of diffraction peaks are based on the following PDF numbers: γ-alumina (PDF#10-0425), $AlVMoO_7$ (PDF#46-0687), $Mo_6V_9O_{40}$ (PDF#34-0527), and MoV_2O_8 (PDF#74-0050).

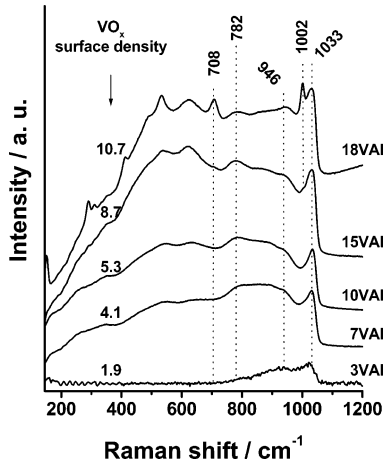

Figure 2. Raman spectra of *x*VAl ($x = 3-18$). Samples were treated in flowing dry air at 673 K for 1 h.

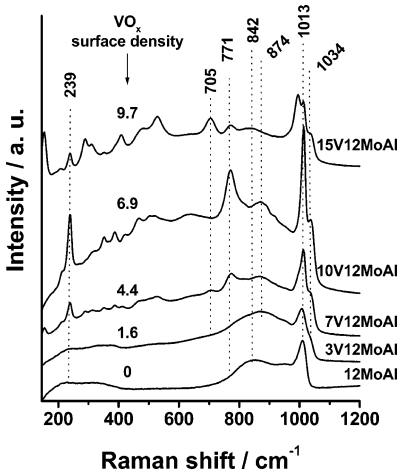

Figure 3. Raman spectra of 12MoAl and *x*V12MoAl ($x = 3-15$) treated in flowing dry air at 673 K for 1 h.

Polyvanadates become evident from emerging bands at 700−1000 cm^{-1} as VO_x surface density increases from 1.9 to 8.7 V/nm^2. Crystalline V_2O_5 was detected at high VO_x surface density (>8 V/nm^2) from its two bands at 1002 and 708 cm^{-1}, consistent with saturation of polyvanadate monolayers at 7−8 V/nm^2.[57] Raman scattering cross sections for bulk V_2O_5 are ~10 times larger than for monovanadates.[58] Thus, dispersed VO_x species remain predominant in 15VAl and 18VAl samples.

Raman spectra for dehydrated 12MoAl and V-coated 12MoAl samples with various VO_x surface densities (*x*V12MoAl, $x = 3-15$; 1.6−9.7 V/nm^2) are shown in Figure 3. 12MoAl showed bands at 1013 and 842 cm^{-1}, attributed to Mo═O and Mo−O−Mo stretches, respectively.[36,59−61] Raman bands for crystalline MoO_3 were not detected on samples prepared using molybdenyl acetylacetonate as the precursor and a surface density of 5.0 Mo/nm^2, corresponding to approximately one monolayer.[62] In contrast, MoAl samples prepared with ammonium heptamolybdate showed crystalline MoO_3 bands at surface densities above 4.5 Mo/nm^2.[36,50] Only a small unresolved band at 1034 cm^{-1}, assigned to V═O stretches, appeared when VO_x was deposited on 12MoAl at low surface densities (Figure 3, 3V12MoAl; 1.6 V/nm^2). Higher VO_x surface densities led to two new bands at 771 and 239 cm^{-1}, together with a more intense band at 1013 cm^{-1}, which was also present in the spectrum for 12MoAl. The 771 cm^{-1} band was previously assigned to Mo−O−V stretches in molybdovanadates.[50,51] The intensities for the bands at 1013, 771, and 239 cm^{-1} change to similar extents with increasing VO_x surface density; thus, they appear to arise from a common V−Mo oxo-structure containing V−O−Mo linkages. A definitive assignment is not possible, but their sharp nature and concurrent appearance with $AlMoVO_7$ diffraction lines in 10V12MoAl (Figure 1) suggest that they arise from this crystalline phase. The 10V12MoAl sample, which contains an equivalent VO_x monolayer on Al_2O_3 precoated with a similar equivalent MoO_x monolayer, showed the most intense bands at 1013, 771, and 239 cm^{-1} (Figure 3), consistent with intimate mixing between VO_x and MoO_x species. Raman bands at 705 and 1002 cm^{-1} for crystalline V_2O_5 were detected at VO_x surface densities of 9.7 V/nm^2 (15V12MoAl).

Raman spectra for 10V*x*MoAl ($x = 4-20$) samples, which contain an equivalent VO_x monolayer on Al_2O_3 supports modified by varying amounts of MoO_x, are shown in Figure 4. Raman spectra for 10V4MoAl (Figure 4) and 10VAl (Figure 2) are similar. Bands at 1013, 771, and 239 cm^{-1}, corresponding to V−Mo−(Al)−O phases, were detected as MoO_x surface density increased; these bands reached maximum intensities for 10V12MoAl, which contains equivalent monolayers of both VO_x and MoO_x components. Diffraction patterns suggest here also that these new bands arise from crystalline $AlVMoO_7$ structures. Crystalline MoO_3 was detected at surface densities above 6.9 Mo/nm^2. The 1043 cm^{-1} band for V═O stretching modes in monovanadates and polyvanadates decreased monotonically with

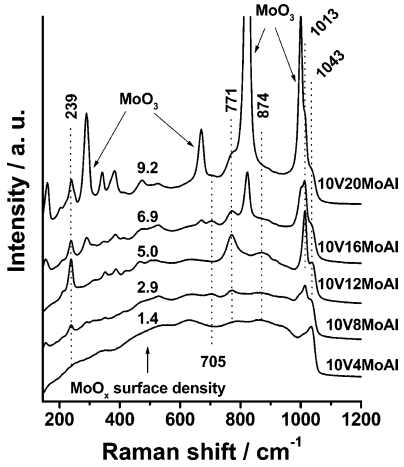

Figure 4. Raman spectra of 10V*x*MoAl ($x = 4-20$) catalysts treated in flowing dry air at 673 K for 1 h.

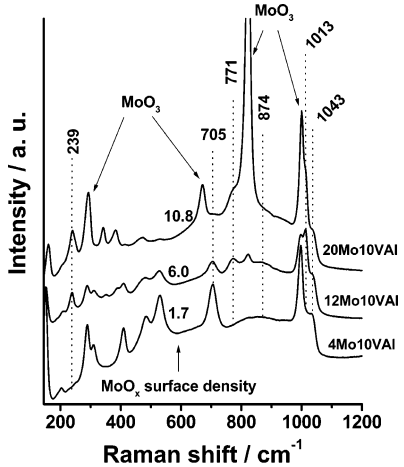

Figure 5. Raman spectra of *x*Mo10VAl ($x = 4-20$) samples treated in flowing dry air at 673 K for 1 h.

increasing MoO_x surface density. Traces of crystalline V_2O_5 were detected on 10V8MoAl and 10V16MoAl. The residual coexistence of crystalline V_2O_5 and MoO_3 in 10V16MoAl indicates that V−Mo−O phases form more readily from dispersed MoO_x and VO_x than from crystalline V_2O_5 and MoO_3 at this treatment temperature.

MoO_x species were supported on Al_2O_3 precoated with an equivalent VO_x monolayer in an effort to explore the effects of deposition sequence on the structure and function of dispersed binary oxides. Figure 5 shows that a mixed V−Mo−O phase is present in 12Mo10VAl and 20Mo10VAl (bands at 1013, 771, and 239 cm^{-1}), but its characteristic bands are less intense than for similar compositions prepared via the reverse sequence (Figure 4; 10V12MoAl). Crystalline V_2O_5 was detected in 4Mo10VAl and 12Mo10VAl, possibly because of the detachment and recrystallization of dispersed VO_x structures during subsequent impregnation with MoO_x precursors. As MoO_x surface densities exceed one equivalent MoO_x monolayer in 20Mo10VAl, intense bands appear at 1000, 823, 680, and 320 cm^{-1}, corresponding to crystalline MoO_3.

Figure 6 shows Raman spectra for 12CrAl and *x*V12CrAl ($x = 3-15$; 2.1−9.5 V/nm^2) samples, which contain an equivalent CrO_x monolayer (7.9 Cr/nm^2).[63] Polychromates, with Raman bands at 750−900 cm^{-1}, are the predominant structures for CrO_x species supported on pure Al_2O_3, especially at CrO_x surface densities above 3 Cr/nm^2.[55,56,64,65] The 12CrAl sample shows three intense bands at 1009, 879, and 799 cm^{-1}. The 1009 cm^{-1}

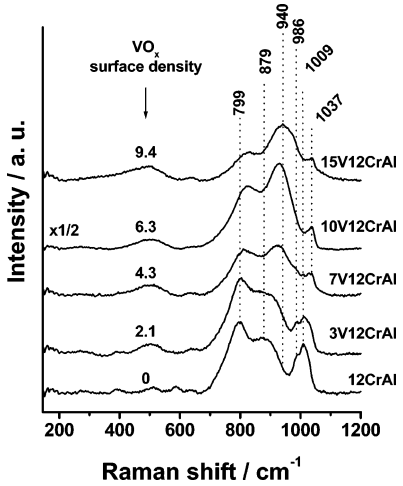

Figure 6. Raman spectra of 12CrAl and *x*V12CrAl ($x = 3-15$) treated in flowing dry air at 673 K for 1 h.

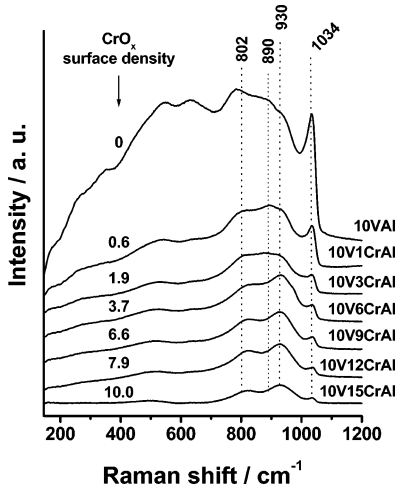

Figure 7. Raman spectra of 10VAl and 10V*x*CrAl ($x = 1-15$) treated in flowing dry air at 673 K for 1 h.

band arises from symmetric stretches in the O═Cr═O group within chromates, while the 879 and 799 cm^{-1} bands reflect Cr−O−Cr stretches in dichromates and trichromates, respectively.[56,64] The weak band at 986 cm^{-1} is assigned to CrO_3 (bands at 975 and 495 cm^{-1}),[56] but crystalline Cr_2O_3 (with a band at 550 cm^{-1}) was not detected in any of the samples.[39,56]

Raman bands at 1009, 986, 879, and 799 cm^{-1} weakened upon addition of VO_x to 12CrAl samples and were ultimately replaced by a band at 1037 cm^{-1} assigned to V═O stretches and by two broad bands at 940 and 820 cm^{-1}. The broad nature of these two latter bands suggests that they arise from well-dispersed structures. Definitive assignment of the band at 940 cm^{-1} is not possible. It appears at a frequency similar to that for orthorhombic $CrVO_4$ (924 cm^{-1}),[66,67] but the absence of corresponding diffraction lines suggests that it exists as disordered and highly dispersed $CrVO_4$ domains, which tend to form at low temperature.[68−70] The origin of the 830 cm^{-1} band is unclear; it may reflect the presence of polychromates, polyvanadates, or mixed V−O−Cr oligomers. Crystalline V_2O_5 was not detected, even at the highest VO_x surface density (15V12CrAl; 9.4 V/nm^2).

Figure 7 shows Raman spectra for 10VAl and 10V*x*CrAl ($x = 1-15$) samples with an equivalent VO_x monolayer dispersed on CrAl supports at varying CrO_x surface densities. The relative intensities of bands at 700−1000 cm^{-1} change with increasing Cr content. Bands at 786 and 890 cm^{-1} in 10VAl became

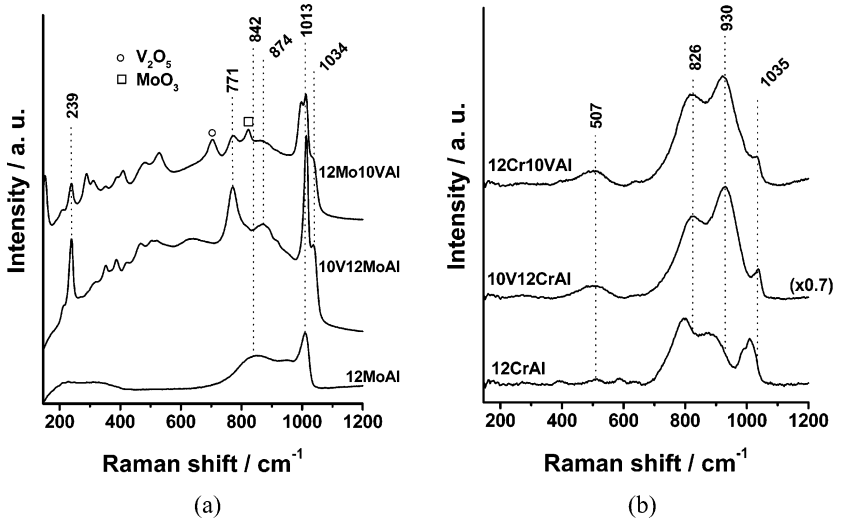

Figure 8. Raman spectra of (a) 12MoAl, 10V12MoAl, and 12MoVAl and (b) 12CrAl, 10V12CrAl, and 12Cr10VAl.

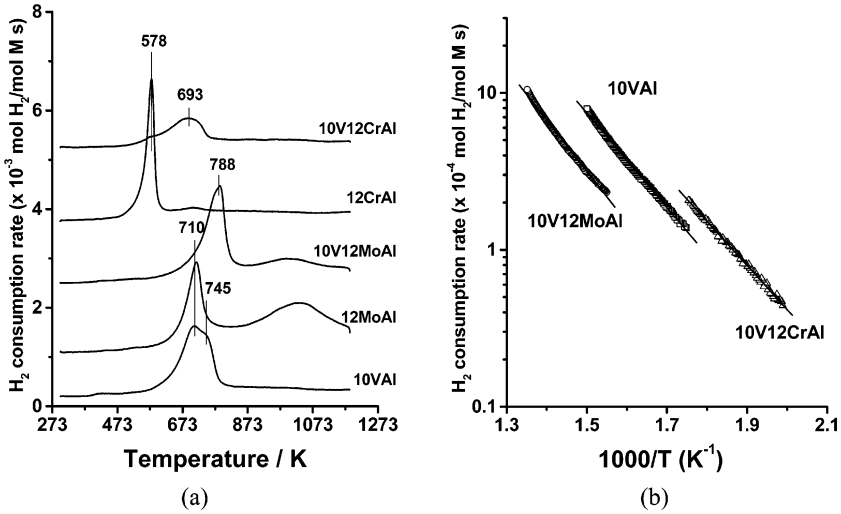

Figure 9. (a) TPR profiles of 10VAl, 12MoAl, 10V12MoAl, 12CrAl, and 10V12CrAl catalysts and (b) Arrhenius plots of the initial rate of H_2 consumption during TPR.

weaker, while the 930 cm^{-1} band became stronger, possibly due to $CrVO_4$ formation. Only the 820 and 930 cm^{-1} bands remained at CrO_x surface densities above 3.7 Cr/nm^2. The replacement of multiple bands for polyvanadates in 10VAl (Figure 2) with two bands at 820 and 930 cm^{-1} in *x*V12CrAl ($x = 7-15$) suggests that VO_x species formed $CrVO_4$ species or dispersed more uniformly on $CrO_x-Al_2O_3$ than on pure Al_2O_3 supports.

Raman spectra for 12MoAl, 10V12MoAl, and 12Mo10VAl and those for 12CrAl, 10V12CrAl, and 12Cr10VAl are compared in Figure 8a and b. Mixed Mo−O−V structures were detected on both 10V12MoAl and 12Mo10VAl. The spectra for 10V12CrAl and 12Cr10VAl are very similar, suggesting that the binary dispersed oxide structures formed are essentially independent of deposition sequence. Both spectra show a band at 930 cm^{-1}, similar to that observed in $CrVO_4$ (924 cm^{-1}).[66,67]

3.1.2. Reduction of the Catalysts. Figure 9a shows reduction profiles for 10VAl, 12MoAl, 10V12MoAl, 12CrAl, and 10V12CrAl. The 10VAl sample shows a peak at 710 K with a shoulder at 745 K, previously assigned to reduction of V^{5+} to V^{3+} in various polyvanadates,[23,50] and consistent with multiple Raman bands at 700−1000 cm^{-1} in 10VAl (Figure 2). The 12MoAl sample shows a peak at 716 K, attributed to Mo^{6+} reduction to Mo^{4+} in dispersed MoO_x, and another peak at 1033 K, corresponding to Mo^{4+} reduction to Mo^0.[23,50,71] The H_2/Mo ratios for the reduction peaks at 716 and 1033 K are 0.86 and 2.02, respectively, consistent with their respective assignments.

The reduction profile for 10V12MoAl also shows two peaks; the first peak (788 K) is attributed to the simultaneous reduction of Mo^{6+} and V^{5+} in V−Mo−O structures to Mo^{4+} and V^{3+}, respectively, while the peak at 1000 K reflects the reduction of Mo^{4+} to Mo^0. The reduction profiles for 10V12MoAl and 12Mo10VAl are very similar (Figure 10a) except for a slightly lower temperature for the first reduction peak in 12Mo10VAl (760 vs 786 K). Table 4 lists the assignments of each reduction peak and the moles of H_2 consumed per mole of metal. This table also shows the expected (stoichiometric) consumption of H_2 in each case. Measured H_2 consumption ratios are very similar to those expected for each reduction peak and for the total extent of reduction in 12MoAl, 10VAl, 10V12MoAl, and 12Mo10VAl samples.

Reduction profiles for 12CrAl and 10V12CrAl are shown in Figure 9a; their interpretation is more complex than from Mo−V systems, because of the tendency of CrO_x structures to autoreduce to various extents during thermal treatments. The peak at 578 K for 12CrAl corresponds to reduction of Cr^{6+} to Cr^{3+}.[39,40] Table 4 shows, however, that measured H_2 consumptions for reduction of CrO_x species are smaller than expected for the reduction of all Cr atoms in the sample from Cr^{6+} to Cr^{3+}, suggesting that only ~60% of Cr cations exist as Cr^{6+} in 12CrAl

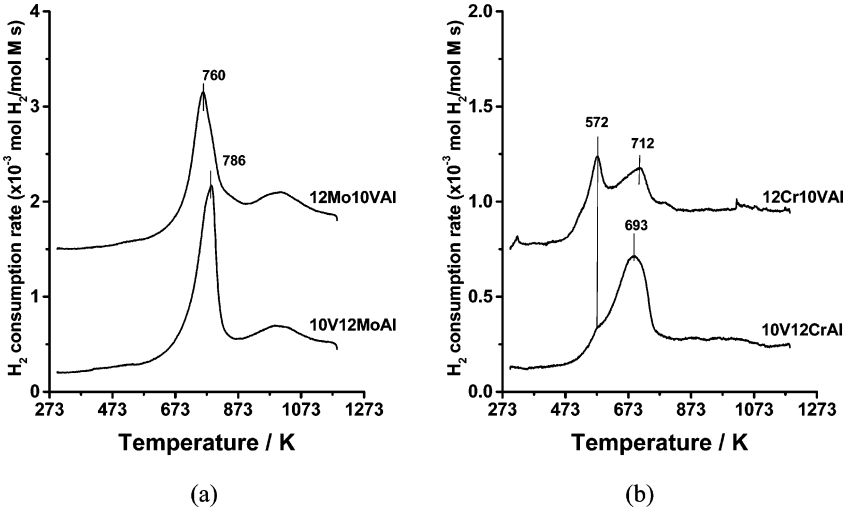

Figure 10. Comparison of TPR profiles for (a) 10V12MoAl and 12Mo10VAl and (b) 10V12CrAl and 12Cr10VAl.

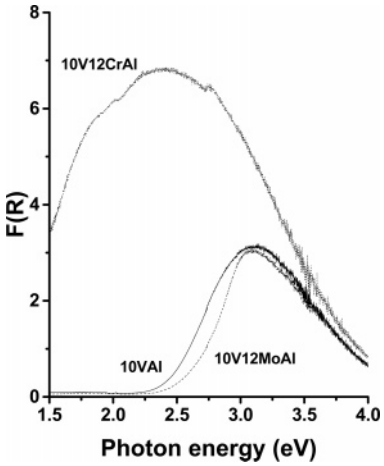

Figure 11. UV−visible spectra of 10VAl, 10V12MoAl, and 10V12CrAl treated at 723 K in flowing dry air for 0.5 h.

after thermal treatment in air. This proposal was confirmed by the fraction of the Cr as Cr^{6+} in *x*CrAl ($x = 1-12$) (see Figure A of Supporting Information); in these samples, the fraction of the Cr as Cr^{6+} decreased monotonically from unity to 0.6 as *x* increased from 1 to 12 (i.e., 0.5−8 Cr/nm^2). Oxide supports stabilize surface chromate species in hexavalent form, but Cr atoms in excess of those required for a polychromate monolayer form a three-dimensional structure that reduces to trivalent species to form Cr_2O_3 during thermal treatment in air.[64,72−74] Our findings indicate that such Cr^{3+} structures start to form at CrO_x surface densities above >2 Cr/nm^2.

TABLE 4: Assignments of TPR Results Reported in Figures 9 and 10

sample	reduction peak temperature (K)	assignment	H_2/M (M = V, Mo, or Cr) (theoretical values are given in parentheses)
10VAl	710−745	$V^{5+} \rightarrow V^{3+}$	0.92 (H_2/V = 1)
12MoAl	710	$Mo^{6+} \rightarrow Mo^{4+}$	0.86 (H_2/Mo = 1)
	1053	$Mo^{4+} \rightarrow Mo^{0}$	2.02 (H_2/Mo = 2)
12CrAl	578	$Cr^{6+} \rightarrow Cr^{3+}$	0.91 (H2/Cr = 1.5)
10V12MoAl	786	$V^{5+} \rightarrow V^{3+}$	0.99 (H_2/(V + Mo) = 1)
		$Mo^{6+} \rightarrow Mo^{4+}$	
	1053	$Mo^{4+} \rightarrow Mo^{0}$	1.9 (H_2/Mo = 2)
12Mo10VAl	760	$V^{5+} \rightarrow V^{3+}$	0.89 (H_2/(V + Mo) = 1)
		$Mo^{6+} \rightarrow Mo^{4+}$	
	1053	$Mo^{4+} \rightarrow Mo^{0}$	2.1 (H_2/Mo = 2)
10V12CrAl	572	$Cr^{6+} \rightarrow Cr^{3+}$	0.12 (H_2/Cr = 1.5)
	693	$V^{5+} \rightarrow V^{3+}$	1.08 (H_2/V = 1)
12Cr10VAl	572	$Cr^{6+} \rightarrow Cr^{3+}$	0.29 (H_2/Cr = 1.5)
	712	$V^{5+} \rightarrow V^{3+}$	0.91 (H_2/V = 1)

The 10V12CrAl samples show two overlapping reduction features at 578 and 693 K, which were assigned to CrO_x and VO_x reduction, respectively. The CrO_x reduction peak in 10V12CrAl appears as a small shoulder next to the VO_x reduction peak, even though the number of lattice oxygens associated with VO_x and CrO_x in this sample are similar, indicating that the fraction of the Cr atoms as Cr^{6+} in 10V12CrAl is significantly smaller than that in 12CrAl. In contrast, all V^{5+} reduce to V^{3+} in this sample. These data indicate that the deposition of a nominal monolayer of VO_x on 12CrAl leads to the reaction of most CrO_x species with VO_x to form dispersed $CrVO_4$ during thermal treatment.

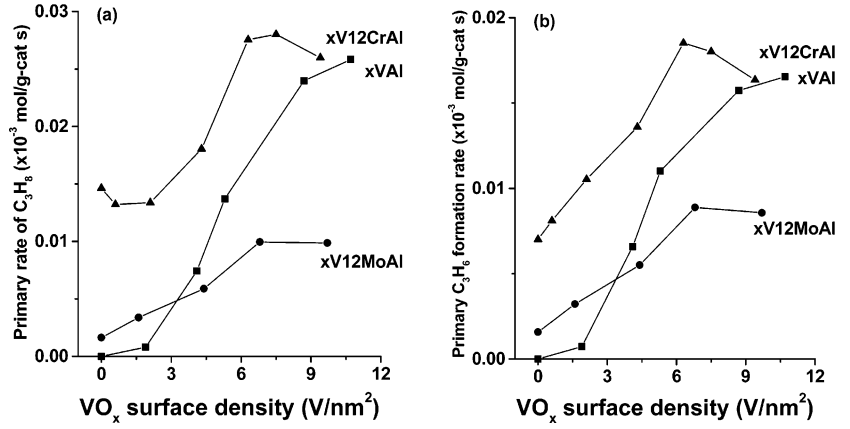

Figure 12. Weight-based activity of *x*VAl, *x*V12MoAl, and *x*V12CrAl for (a) C_3H_8 consumption and (b) C_3H_6 formation.

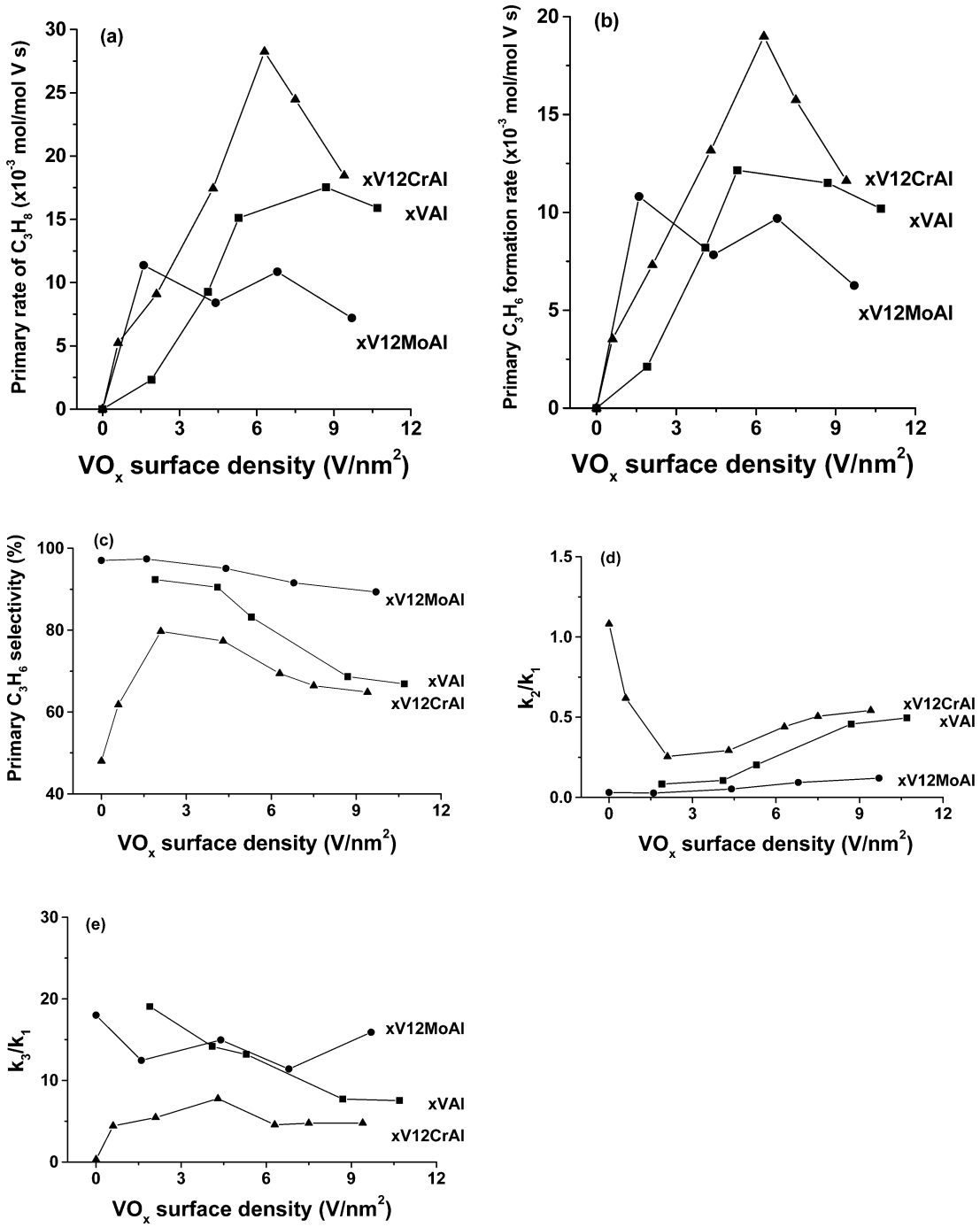

Figure 13. Effect of VO_x surface density on the reactivity of VAl, VmoAl, and VCrAl at 673 K: (a) primary rate of propane consumption; (b) primary rate of propene formation; (c) primary selectivity to propene; (d) k_2/k_1 and (e) k_3/k_1. Reaction conditions: $P_{C_3H_8} = 13.5$ kPa, $P_{O_2} = 1.7$ kPa.

Reduction profiles for 12Cr10VAl and 10V12CrAl (Figure 10b) show that the CrO_x reduction peak at 572 K is smaller in the latter sample. Consistent with this, Table 4 shows that the fraction of the Cr atoms present as Cr^{6+} is higher in 12Cr10VAl than in 10V12CrAl; this indicates that 12Cr10VAl contains a smaller fraction of the CrO_x as $CrVO_4$ than 10V12CrAl. This may be the reason that the reactivity of 12Cr10VAl is more similar to 12CrAl rather than 10VAl, as we report in the next section. The reduction profiles in Figure 9a indicate that VO_x species reduce faster in 10V12CrAl than in 10VAl, while the MoO_x layer in 10V12MoAl leads to slower VO_x reduction than in 10VAl. Arrhenius plots of the initial H_2 consumption rates obtained during the early stages of the stoichiometric reduction of these oxides in H_2 (<15% reduction) are shown in Figure 9b. The initial H_2 consumption rates in 10V12CrAl are higher than in 10VAl at all temperatures, while rates in 10V12MoAl are lower than in VAl. We expect and indeed find significant catalytic consequences of these reducibility trends for oxidative dehydrogenation reactions, as we discuss below.

3.1.3. UV−Visible Characterization. UV−visible spectra are shown in Figure 11 for 10VAl, 10V12MoAl, and 10V12CrAl. The spectra for 10VAl and 10V12MoAl are similar and show an absorption feature at 3.1 eV, while 10V12CrAl shows more intense absorption features, including two at 1.8 and 2.5 eV, corresponding to d−d transitions in Cr^{3+} centers and charge transfer in polychromates,[39,64] without detectable spectral contributions from V^{5+}.

UV−visible edge energies for 10VAl and 10V12MoAl samples are 2.25 and 2.40 eV, respectively. A previous study[23] reported that ODH turnover rates increased with decreasing

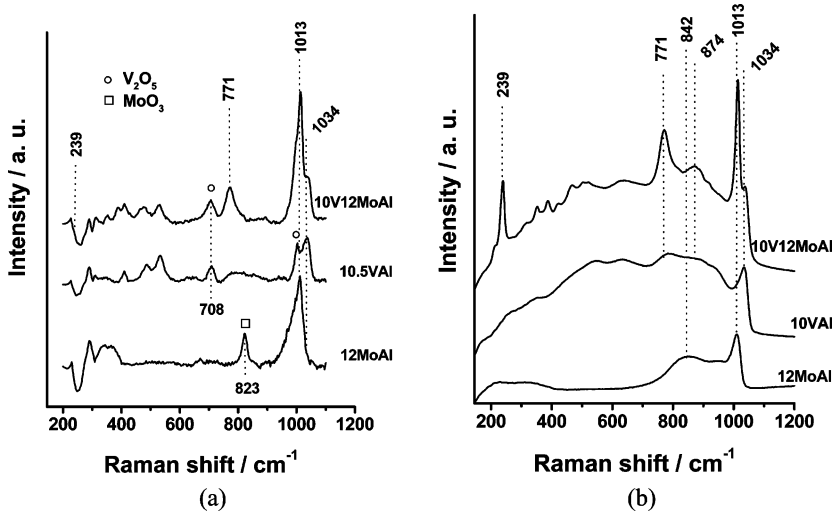

Figure 14. Comparison of Raman spectra for 12MoAl, 10Val, and 10V12MoAl reported by Dai et al.[50] and those reported here.

absorption edge energy; thus, 10VAl would be expected to show lower ODH rates than 10V12MoAl, as found experimentally and reported below. The 10V12CrAl sample does not show an absorption edge, apparently because it occurs below 1.5 eV.

In summary, Raman, reduction, and UV−visible data indicate that polyvanadate structures predominate in VAl samples. Mixed metal oxides form when MoO_x is placed below or above VO_x, which leads to less reducible oxides and to higher absorption edge energies than in VAl. Raman and reduction results also show that most CrO_x species react with VO_x to form $CrVO_4$ when VO_x is deposited over a nominal CrO_x monolayer on Al_2O_3, but that some CrO_x remains unreacted when it is deposited over a nominal monolayer of VO_x on Al_2O_3.

3.2. Oxidative Dehydrogenation Rates and Selectivities. Rates normalized by catalyst mass are shown in Figure 12 for C_3H_8 conversion and C_3H_6 formation on *x*VAl, *x*V12MoAl, and *x*V12CrAl as a function of VO_x surface density. As reported previously,[22] ODH rates on *x*VAl increase with increasing VO_x surface density and reach constant values at ~7 V/nm^2. These trends reflect the higher VO_x content and specific reactivity with increasing surface density, as more reactive polyvanadates replace less active and reducible monovanadate structures.[23]

VO_x surface density effects on primary ODH rates (per V-atom) and selectivities and on rate constant ratios are shown in Figure 13 for *x*VAl, *x*V12MoAl, and *x*V12CrAl. For *x*V12MoAl and *x*V12CrAl, catalytic contributions from the part of the surface not covered by VO_x species were subtracted from measured rates and residual VO_x contributions were normalized by the V-atoms in each sample. This procedure assumes that the fraction of the support covered by VO_x is proportional to VO_x surface density up to 7 V/nm^2 and that exposed Mo- and Cr-coated surfaces catalyze reactions with rates similar to those on 12MoAl and 12CrAl samples.

Primary rates for propane conversion and propene synthesis increased with increasing VO_x surface density and reached maximum values at ~7 V/nm^2 on *x*VAl (Figure 13a and b), corresponding to an equivalent polyvanadate monolayer, as reported previously.[22] This trend reflects the higher reactivity of oligomeric VO_x species relative to VO_x monomers as the VO_x coverage increases and is consistent with a concurrent decrease in absorption-edge energies and an increase in the rate of stoichiometric VO_x reduction with H_2.

Figure 13d and e shows that k_2/k_1 ratios increase and k_3/k_1 ratios decrease with increasing VO_x surface density on *x*VAl. These trends reflect the increasing propensity for propane to undergo combustion as the surface of alumina is covered by vanadia, and the tendency for propene to react less readily with increasing vanadia coverage. The latter trend is a consequence of the reduction in exposed alumina surface, on which are present Br*ϕ*nsted acid sites. A decrease in the exposure of such sites to the gas phase lowers the ease of readsorption of the newly formed olefin.

Effects of VO_x surface density on primary ODH rates (per V-atom) are also observed on *x*V12MoAl and *x*V12CrAl. At low VO_x surface densities (<3 V/nm^2), rates on *x*V12MoAl and *x*V12CrAl are similar and higher than on *x*VAl. At higher VO_x surface densities, rates on *x*V12MoAl become lower than on *x*VAl. This behavior appears to reflect the mixing of V and Mo species, leading to the replacement of V−O−V structures with less reactive V−O−Mo structures. Below 3 V/nm^2, monovanadates prevail on both Al_2O_3 and 12MoAl surfaces (Figure 3) and V−O−Al species in *x*VAl are thus replaced, at least in part, by V−O−Mo, leading to greater reducibility and ODH reaction rates. Above 3 V/nm^2, polyvanadates form on *x*VAl, while mixed oxides form on *x*V12MoAl, leading to a net replacement of more reactive V−O−V species with less reactive V−O−Mo structures. Thus, active catalytic structures in polyvanadates are rendered less active by dilution with Mo−oxo linkages. This interpretation is consistent with the lower reduction rates and higher reduction peak temperature in 10V12MoAl than on 10VAl for samples containing predominantly polyvanadate and oligomeric Mo−O−V structures (Figure 9).

These effects of mixed VO_x and MoO_x structures differ from those reported previously;[50] that study reported that 10V12MoAl shows higher ODH rates (per V-atom) than 10VAl. These differences reflect the use of different VO_x precursors used to prepare 10VAl (ammonium metavanadate) and 10V12MoAl (vanadyl isopropoxide) in the previous study.[50] Figure 14 shows Raman spectra for 12MoAl, 10.5VAl, and 10V12MoAl reported previously[50] and for identical compositions prepared by the methods used here (see Experimental Section). The use of ammonium heptamolydate and ammonium metavanadate as precursors led to low MoO_x and VO_x dispersions on alumina, as evidenced by the appearance of bands for MoO_3 and V_2O_5 in these samples.[50] The bands for oligomeric MoO_x and VO_x are also less intense than those observed in the samples prepared for the present study. On the other hand, the samples of 10V12MoAl prepared previously[50] exhibit a Raman spectrum

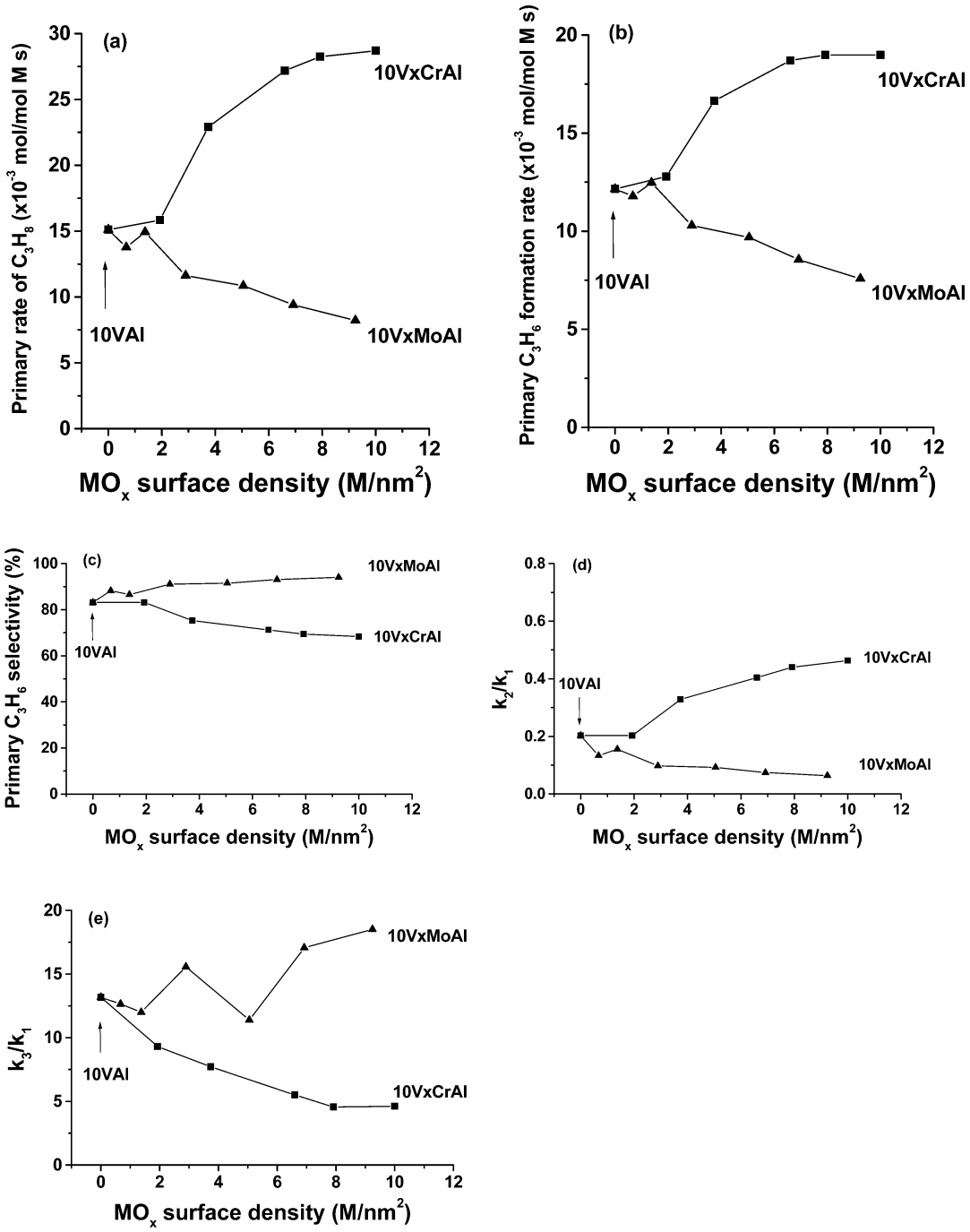

Figure 15. Effect of MoO_x and CrO_x surface density on the reactivity of VMoAl and VCrAl at 673 K: (a) primary rate of propane consumption; (b) primary rate of propene formation; (c) primary selectivity to propene; (d) k_2/k_1 and (e) k_3/k_1. Reaction conditions: $P_{C_3H_8} = 13.5$ kPa, $P_{O_2} = 1.7$ kPa.

very similar to that reported here, with clear evidence for Mo−O−V structures (1013, 771, and 239 cm^{-1} bands). Thus, the higher ODH rates (per V-atom) reported earlier for 10V12MoAl relative to 10VAl are due predominantly to differences in synthetic methods. The results and conclusions in the present study are consistent with those of Bañares and Khatib,[51] who found no synergistic effects in VO_x-MoO_x/Al_2O_3 samples prepared by coimpregnation of V and Mo precursors.

Figure 13d shows that k_2/k_1 values are much lower on *x*V12MoAl than on *x*VAl, especially for VO_x surface densities above 5 V/nm^2. Values of k_3/k_1 are lower on *x*V12MoAl than on *x*VAl for VO_x surface densities below 4 V/nm^2, but these trends are reversed at higher VO_x surface densities. At low surface densities, these effects reflect the coverage of MoO_x species by more selective VO_x domains, as shown by the higher value of k_3/k_1 measured for a MoO_x monolayer on Al_2O_3 than for a similar VO_x monolayer (Figure 13e). Thus, partial coverage of 12MoAl surfaces by VO_x would lead to the observed initial decrease in k_3/k_1 values with increasing surface density in *x*V12MoAl samples. These effects are ultimately reversed as mixing of the VO_x and MoO_x structures occurs with increasing VO_x surface density, a process that leads to higher k_3/k_1 ratios.

Primary ODH rates (per V-atom) on *x*V12CrAl exceed those on *x*VAl, even after subtracting contributions from exposed 12CrAl surfaces, at all VO_x surface densities (Figure 13). Both Raman spectra and reduction profiles for *x*V12CrAl indicate that VO_x increases the fraction of CrO_x that forms $CrVO_4$.

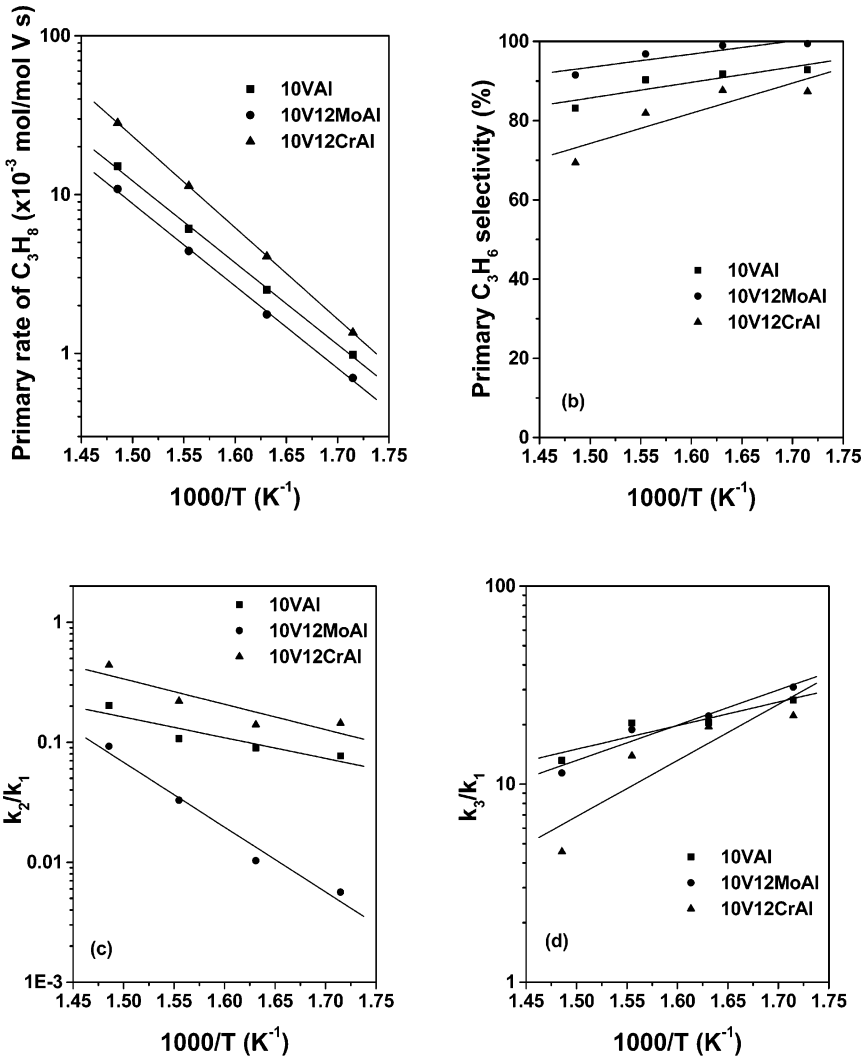

Figure 16. Comparison of the effects of temperature on the reactivity of 10VAl, 10V12MoAl, and 10V12CrAl: (a) primary rate of propane consumption; (b) primary selectivity to propene; (c) k_2/k_1 and (d) k_3/k_1. Reaction conditions: $P_{C_3H_8} = 13.5$ kPa, $P_{O_2} = 1.7$ kPa.

Therefore, the higher specific ODH rates per V-atom of *x*V12CrAl relative to *x*VAl are attributed to the formation of V−O−Cr structures, which replace V−O−Al sites at low VO_x surface densities. The value of k_2/k_1 on 12CrAl (1.1) is higher than on 10VAl (0.2) and decreases with increasing VO_x surface density up to 3 V/nm^2 (Figure 13d). Above this V-content, k_2/k_1 increases with VO_x surface density as in *x*VAl samples. Thus, the blocking of CrO_x oligomers, with high propane combustion reactivity, by VO_x reduces their contribution to combustion pathways, presumably because an increasing fraction of exposed surfaces consist of VO_x or $VCrO_x$ domains. In contrast, values of k_3/k_1 are very low on 12CrAl, and VO_x deposition leads to higher values at low VO_x surface densities, but ultimately to a decrease similar to that observed on *x*VAl as $VCrO_x$ species form with increasing surface density.

The interpretations of the effects of MoO_x and CrO_x underlayers on the structure and catalytic properties of VO_x domains presented above are consistent with the data in Figure 15 for samples in which an equivalent VO_x monolayer is deposited onto an Al_2O_3 surface partly or fully covered by MoO_x or CrO_x. Partial MoO_x coverages decreased ODH rate (per V-atom) because Mo−O−V bonds are less reactive than the V−O−V bonds prevalent in 10VAl at these VO_x surface densities. With increasing MoO_x surface density, k_2/k_1 decreases and k_3/k_1 increases. This is consistent with the lower k_2/k_1 values and higher k_3/k_1 ratios on MoO_x than VO_x domains (Figure 13). Partial coverage of Al_2O_3 by CrO_x leads to effects opposite to those observed for equivalent MoO_x coverages. ODH rates (per V-atom) increased monotonically, while k_2/k_1 increased and k_3/k_1 decreased, with increasing CrO_x surface density.

Temperature effects on propane consumption, propene selectivity, and k_2/k_1 and k_3/k_1 ratios are shown in Figure 16 for similar VO_x monolayers in 10VAl, 10V12MoAl, and 10V/12CrAl. At all temperatures, the rate of propane conversion is higher for VO_x dispersed on 12CrAl than on Al_2O_3, while VO_x deposited onto 12MoAl leads to lower rates than on Al_2O_3. Propene selectivities are highest on 10V12MoAl and lowest on 10V12CrAl, with 10VAl giving intermediate values. On all three catalysts, propane consumption rates increased and propene selectivities decreased with increasing temperature; the latter reflects the observed increase in k_2/k_1 with temperature, which arises from slightly higher activation energy for combustion than for dehydrogenation of propane. In contrast, k_3/k_1 decreases markedly with increasing temperature, as expected from the lower activation energies involved in cleaving allylic C−H groups in propene as compared to those required for activation of stronger methylene C−H bonds in propane.[19] Temperature effects on k_2/k_1 are stronger on 10V12MoAl than on 10VAl or 10V12CrAl samples, but temperature effects on k_3/k_1 are more marked on 10V12CrAl than on 10VAl or 10V12MoAl.

The extent of mixing between an equivalent VO_x monolayer and supports coated with MoO_x or CrO_x monolayers was probed

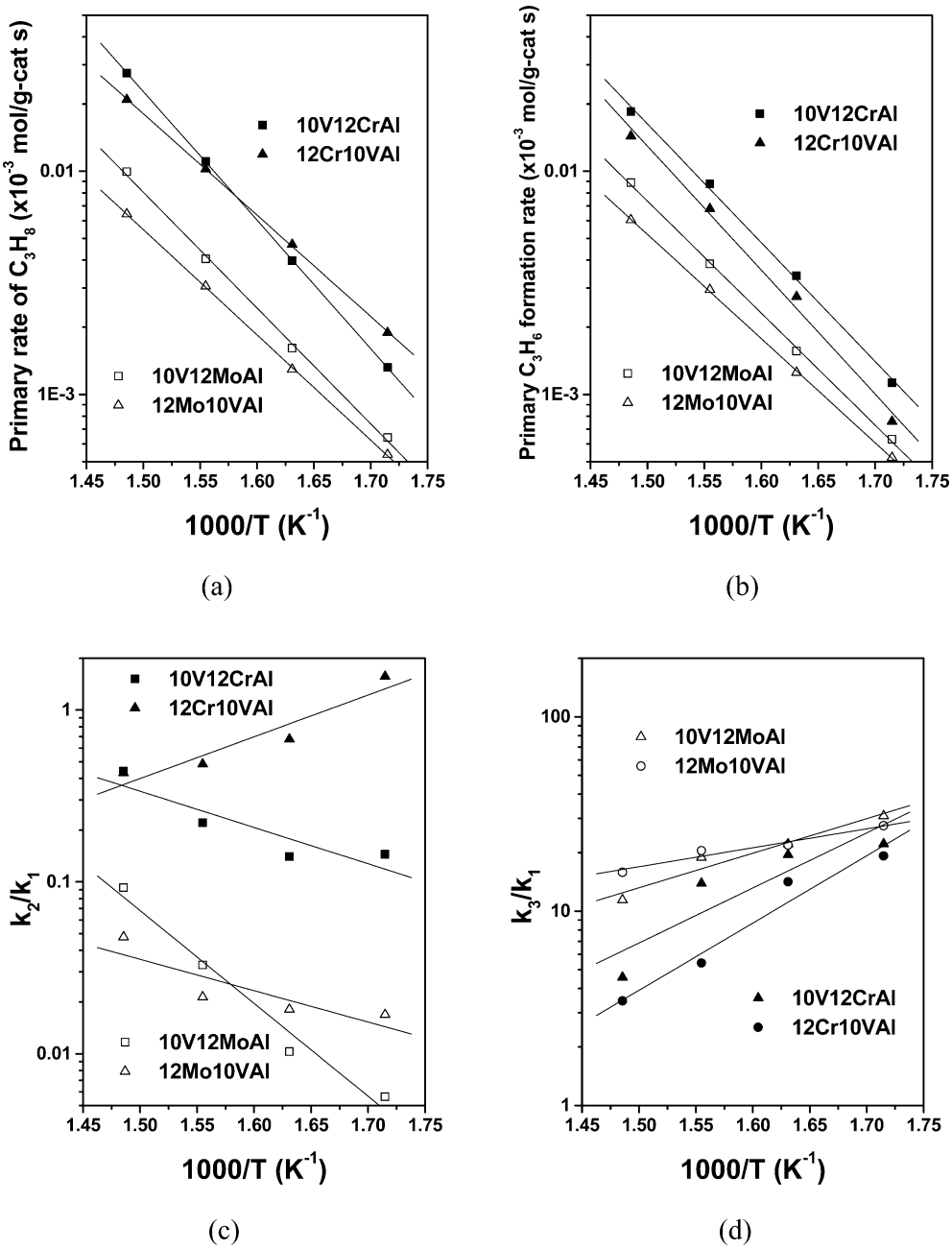

Figure 17. Comparison of the effects of temperature on the reactivity of 10V12MoAl, 12Mo10VAl, 10V12CrAl, and 12Cr10VAl: (a) primary rate of propane consumption; (b) primary selectivity to propene; (c) k_2/k_1 and (d) k_3/k_1. Reaction conditions: $P_{C_3H_8} = 13.5$ kPa, $P_{O_2} = 1.7$ kPa.

by reversing the order of layer deposition. The effects of deposition sequence on dehydrogenation rates and on k_2/k_1 and k_3/k_1 ratios are shown as a function of temperature in Figure 17. Dehydrogenation rates (per mass) are 1.3 times higher at 673 K when MoO_x was deposited first. Below 635 K, k_2/k_1 is lower on 10V12MoAl than on 12Mo10VAl, but it becomes larger above 635 K, because of the stronger effects of temperature on k_2/k_1 on the 10V12MoAl sample. Values of k_3/k_1 are very similar on 10V12MoAl and 12Mo10VAl, although the value of k_3/k_1 for 10V12MoAl decreases somewhat more rapidly with increasing temperature. These effects of deposition sequence reflect significant but incomplete mixing between VO_x and MoO_x monolayers. Raman spectra for 10V12MoAl and 12Mo10VAl showed bands for mixed Mo−O−V structures (Figure 8), especially when MoO_x is deposited first (10V12MoAl), but their reduction profiles are very similar (Figure 10). These data, taken together with the observed catalytic consequences of deposition sequence (Figure 17), indicate that significant mixing occurs during deposition or subsequent thermal treatment in VO_x−MoO_x binary dispersed oxide samples. The small remaining catalytic differences between 10V12MoAl and 12Mo10VAl reflect the presence of small amounts of VO_x at 10V12MoAl surfaces and small amounts of MoO_x at 12Mo10VAl surfaces.

For binary dispersed oxide samples containing equivalent monolayers of VO_x and CrO_x, the rate of propane ODH (per mass) is 1.5 times higher when CrO_x is deposited first (10V12CrAl) instead of VO_x (12Cr10VAl). The effects of temperature on k_2/k_1 are strongly influenced by the sequence of deposition; k_2/k_1 increases with temperature on 10V12CrAl, as was also found on 10VAl, but shows the opposite trend on 12Cr10VAl, as was also observed on 12CrAl. These effects of deposition sequence suggest that the surfaces of these dispersed binary oxides retain some of the properties of the oxide deposited last, even though most VO_x and CrO_x species interact to form mixed oxides, for example, $CrVO_4$. Values of k_3/k_1 are

higher on 10V12CrAl than on 12Cr10VAl and decrease with temperature on both samples. These data also suggest the predominant exposure of the oxide deposited last, because k_3/k_1 values are lower on 12CrAl than on 10VAl (Figure 13), and both samples show a decrease in k_3/k_1 ratios with increasing temperature (10VAl in Figure 16, temperature effects on 12CrAl not shown). These catalytic consequences of deposition order are much stronger than any structural changes detectable in their Raman spectra (Figure 8), from which it is not possible to assess the extent of mixing in 10V12CrAl and 12Cr10VAl. Reduction profiles for these two samples, however, provide definitive evidence for mixing of VO_x and CrO_x components in these samples. The reduction peak at 572 K (Figure 9), attributable to reduction of exposed CrO_x (Figure 8), is more pronounced in 12Cr10VAl than in 10V12CrAl, suggesting that CrO_x is preferentially exposed at the surface of 12Cr10VAl, consistent with the observed catalytic consequences of the deposition sequence.

4. Conclusions

The deposition of vanadia on alumina covered by an equivalent monolayer of molybdena produces well-dispersed VO_x domains at low V surface densities and results in the formation of a mixed metal oxide ($AlMoVO_4$) at higher V surface densities. This mixed metal oxide is less readily reducible than the polyvandate species that form on the surface of alumina at an equivalent monolayer coverage. For V surface densities below 3 V/nm^2, the specific activity of VMoAl catalysts for propane ODH is higher than that of VAl catalysts, but above this surface coverage the reverse relationship is observed. The ratio of the rate coefficients for propane combustion to ODH (k_2/k_1) is significantly lower for VMoAl catalysts than for VAl catalysts, but the ratio of rate coefficients for propene combustion to propane ODH (k_3/k_1) is more nearly comparable. No significant difference in structure or catalytic activity and selectivity was observed when the order of molybdena and vanadia deposition was reversed, suggesting that the two active oxides are intimately mixed. Deposition of vanadia on alumina covered by an equivalent monolayer of chromia produced well-dispersed $CrVO_4$ species at all vanadia surface coverages. The reducibility of an equivalent monolayer of vanadia dispersed on the chromia-coated alumina is higher than that for an equivalent monolayer of vanadia on alumina. The propane ODH activity of such VCrAl catalysts is higher than that for VAl catalysts at all surface concentrations of vanadia. While the ratio of rate coefficients for propane combustion to ODH (k_2/k_1) is larger for VCrAl catalysts than for VAl catalysts, the ratio of the rates coefficients for propene combustion to propane ODH (k_3/k_1) is much lower for the former catalysts. For VCrAl catalysts, the order of deposition of the components affected the catalytic properties of the material formed. This suggests that some of the component last deposited on the surface remains not fully mixed with the component first deposited. The results of this study demonstrate the relationships between the structure and reactivity of binary dispersed oxides of vanadia and molybdena and of vanadia and chromia and illustrate strategies that can be used to prepare more active and selective alkane ODH catalysts.

Acknowledgment. This work was supported by the Director, Office of Basic Energy Sciences, Chemical Sciences Division of the U.S. Department of Energy under Contract DE-AC03-76SF00098.

Supporting Information Available: Figures of the percentage of Cr as Cr^{6+} in *x*CrAl, *x*V12CrAl, and 12Cr10VAl catalysts. This material is available free of charge via the Internet at http://pubs.acs.org.

References and Notes

(1) Ross, J. R. H.; Smits, R. H. H.; Seshan, K. *Catal. Today* **1993**, *16*, 503.
(2) Kung, H. H. *Adv. Catal.* **1994**, *40*, 1.
(3) Mamedov, E. A.; Cortés-Corberan, V. *Appl. Catal., A* **1995**, *127*, 1.
(4) Cavani, F.; Trifiro, F. *Catal. Today* **1995**, *24*, 307.
(5) Centi, G.; Triffiro, F. *Appl. Catal., A* **1996**, *143*, 3.
(6) Delmon, B.; Ruiz, P.; Carrazan, S. R. G.; Korili, S.; Rodriguez, M. A. Vicente; Sobalik, Z. *Stud. Surf. Sci. Catal.* **1996**, *100*, 1.
(7) Albonetti, S.; Cavani, F.; Trifiro, F. *Catal. Rev.-Sci. Eng.* **1996**, *38*, 413.
(8) Vedrine, J. C.; Millet, J. M. M.; Volta, J.-C. *Catal. Today* **1996**, *32*, 115.
(9) Blasko, T.; López Nieto, J. M. *Appl. Catal., A* **1997**, *157*, 117.
(10) Kung, H. H.; Kung, M. C. *Appl. Catal., A* **1997**, *157*, 105.
(11) Cavani, F.; Trifiro, F. *Catal. Today* **1999**, *51*, 561.
(12) Grasselli, R. K. *Catal. Today* **1999**, *49*, 141.
(13) Bhasin, M. M.; McCain, J. H.; Vora, B. V.; Imai, T.; Pujado, P. R. *Appl. Catal., A* **2001**, *221*, 397.
(14) Sinev, M. Y. *J. Catal.* **2003**, *216*, 468.
(15) Bhasin, M. M. *Top. Catal.* **2003**, *23*, 145.
(16) Khodakov, A.; Yang, J.; Su, S.; Iglesia, E.; Bell, A. T. *J. Catal.* **1998**, *177*, 343.
(17) Khodakov, A.; Olthof, B.; Bell, A. T.; Iglesia, E. *J. Catal.* **1999**, *181*, 205.
(18) Chen, K.; Khodakov, A.; Yang, J.; Bell, A. T.; Iglesia, E. *J. Catal.* **1999**, *186*, 325.
(19) Chen, K.; Bell, A. T.; Iglesia, E. *J. Phys. Chem. B* **2000**, *104*, 1292.
(20) Olthof, B.; Khodakov, A.; Bell, A. T.; Iglesia, E. *J. Phys. Chem. B* **2000**, *104*, 1516.
(21) Chen, K.; Iglesia, E.; Bell, A. T. *J. Catal.* **2000**, *192*, 197.
(22) Argyle, M. D.; Chen, K.; Bell, A. T.; Iglesia, E. *J. Catal.* **2002**, *208*, 139.
(23) Chen, K.; Bell, A. T.; Iglesia, E. *J. Catal.* **2002**, *209*, 35.
(24) Garcia Cortez, G.; Fierro, J. L. G.; Banares, M. A. *Catal. Today* **2003**, *78*, 219.
(25) Grabowski, R.; Sloczynski, J.; Grzesik, N. M. *Appl. Catal., A* **2003**, *242*, 297.
(26) Christodoulakis, A.; Machli, M.; Lemonidou, A. A.; Boghosian, S. *J. Catal.* **2004**, *222*, 293.
(27) Routray, K.; Reddy, K. R. S. K.; Deo, G. *Appl. Catal., A* **2004**, *265*, 103.
(28) Ballarini, N.; Cavani, F.; Cericola, A.; Cortelli, C.; Ferrari, M.; Trifiro, F.; Capannelli, G.; Comite, A.; Catani, R.; Cornaro, U. *Catal. Today* **2004**, *91*−*92*, 99.
(29) Grabowski, R. *Appl. Catal., A* **2004**, *270*, 37.
(30) De, M.; Kunzru, D. *Catal. Lett.* **2004**, *96*, 33.
(31) Pieck, C. L.; Banares, M. A.; Fierro, J. L. G. *J. Catal.* **2004**, *224*, 1.
(32) Chen, K.; Xie, S.; Iglesia, E.; Bell, A. T. *J. Catal.* **2000**, *189*, 421.
(33) Chen, K.; Xie, S.; Bell, A. T.; Iglesia, E. *J. Catal.* **2000**, *195*, 244.
(34) Chen, K.; Iglesia, E.; Bell, A. T. *Stud. Surf. Sci. Catal.* **2001**, *136*, 507.
(35) Chen, K.; Iglesia, E.; Bell, A. T. *J. Phys. Chem. B* **2001**, *105*, 646.
(36) Chen, K.; Xie, S.; Bell, A. T.; Iglesia, E. *J. Catal.* **2001**, *198*, 232.
(37) Abello, M. C.; Gomez, M. F.; Casella, M.; Ferretti, O. A.; Banares, M. A.; Fierro, J. L. G. *Appl. Catal., A* **2003**, *251*, 435.
(38) Heracleous, E.; Lemonidou, A. A.; Lercher, J. A. *Appl. Catal., A* **2004**, *264*, 73.
(39) Cherian, M.; Rao, M. S.; Hirt, A. M.; Wachs, I. E., Deo, G. *J. Catal.* **2002**, *211*, 482.
(40) Cherian, M.; Gupta, R.; Rao, M. S.; Deo, G. *Catal. Lett.* **2003**, *86*, 179.
(41) Cherian, M.; Rao, M. S.; Deo, G. *Catal. Today* **2003**, *78*, 397.
(42) Rao, T. V. M.; Deo, G.; Jehng, J.-M.; Wachs, I. E. *Langmuir* **2004**, *20*, 7159.
(43) Jibril, B. Y.; Al-Zahrani, S. M.; Abasaeed, A. E.; Hughes, R. *Catal. Commun.* **2003**, *4*, 579.
(44) Jibril, B. Y.; Al-Zahrani, S. M.; Abasaeed, A. E.; Hughes, R. *Catal. Lett.* **2003**, *3*−*4*, 121.
(45) Al-Zahrani, S. M.; Jibril, B. Y.; Abasaeed, A. E. *Catal. Lett.* **2003**, *85*, 57.
(46) Jibril, B. Y. *Appl. Catal., A* **2004**, *264*, 193.
(47) Gilardoni, F.; Bell, A. T.; Chakraborty, A.; Boulet, P. *J. Phys. Chem. B* **2000**, *104*, 12250.
(48) Gao, X. T.; Bare, S. R.; Fierro, J. L. G.; Wachs, I. E. *J. Phys. Chem. B* **1999**, *103*, 618.

(49) Liu, H.; Cheung, P.; Iglesia, E. *Phys. Chem. Chem. Phys.* **2003**, *5*, 3795.
(50) Dai, H.; Bell, A. T.; Iglesia, E. *J. Catal.* **2004**, *221*, 491.
(51) Bañares, M. A.; Khatib, S. J. *Catal. Today* **2004**, *96*, 251.
(52) Delgass, W. N. *Spectroscopy in Heterogeneous Catalysis*; Academic Press: New York, 1979.
(53) Barton, D. G.; Shtein, M.; Wilson, R. D.; Soled, S. L.; Iglesia, E. *J. Phys. Chem. B* **1999**, *103*, 630.
(54) Wachs, I. E. *Catal. Today* **1996**, *27*, 437.
(55) Deo, G.; Wachs, I. E. *J. Phys. Chem.* **1991**, *95*, 5889.
(56) Vuurman, M. A.; Wachs, I. E. *J. Phys. Chem.* **1992**, *96*, 5008.
(57) Wachs, I. E.; Weckhuysen, B. M. *Appl. Catal., A* **1997**, *157*, 67.
(58) Xie, S.; Iglesia, E.; Bell, A. T. *Langmuir* **2000**, *16*, 7162.
(59) Chan, S. S.; Wachs, I. E.; Murrell, L. L. *J. Phys. Chem.* **1984**, *88*, 5831.
(60) Hu, H.; Wachs, I. E.; Bare, S. R. *J. Phys. Chem.* **1995**, *99*, 10897.
(61) Mestl, G.; Srinivasan, T. K. K. *Catal. Rev.-Sci. Eng.* **1998**, *40*, 451.
(62) Xie, Y.-C.; Tang, Y.-Q. *Adv. Catal.* **1990**, *37*, 1.
(63) Yang, G.; Haibo, Z.; Biying, Z. *J. Mater. Sci.* **2000**, *35*, 917.
(64) Weckhuysen, B. W.; Wachs, I. E.; Schoonheydt, R. A. *Chem. Rev.* **1996**, *96*, 3327.
(65) Vuurman, M. A.; Stufkens, D. J.; Oskam, A.; Moulijn, J. A.; Kapteijn, F. *J. Mol. Catal.* **1990**, *60*, 83.
(66) Owen, O. S.; Kung, H. H. *J. Mol. Catal.* **1993**, *79*, 265.
(67) Briand, L. E.; Jehng, J.-M.; Cornaglia, L.; Hirt, A. M.; Wachs, I. E. *Catal. Today* **2003**, *78*, 257.
(68) Baran, E. J. *J. Mater. Sci.* **1998**, *33*, 2479.
(69) Baudrin, E.; Denis, S.; Orsini, F.; Seguin, L.; Touboul, M.; Tarascon, J.-M. *J. Mater. Chem.* **1999**, *9*, 101.
(70) Song, Z.; Matsushita, T.; Shishido, T.; Takehira, K. *J. Catal.* **2003**, *218*, 32.
(71) Regalbuto, J. R.; Ha, J.-W. *Catal. Lett.* **1994**, *29*, 189.
(72) Greenwood, N. N.; Earnshaw, A. *Chemistry of the Elements*; Pergamon Press: Elmsford, NY, 1989.
(73) Hardcastle, F. D.; Wachs, I. E. *J. Mol. Catal.* **1988**, *46*, 173.
(74) Vuurman, M. A.; Hardcastle, F. D.; Wachs, *J. Mol. Catal.* **1993**, *84*, 193.